Published in final edited form as:
Mol Microbiol. 2011 July ; 81(2): 340–353. doi:10.1111/j.1365-2958.2011.07616.x.

Mechanisms for maintaining cell shape in rod-shaped Gram-negative bacteria

Leon Furchtgott[1,†], **Ned S. Wingreen**[2], and **Kerwyn Casey Huang**[1,*]

[1]Department of Bioengineering, 318 Campus Drive West, Stanford University, Stanford, CA 94305.

[2]Department of Molecular Biology, Washington Road, Princeton University, Princeton, NJ 08544.

Abstract

For the rod-shaped Gram-negative bacterium *Escherichia coli*, changes in cell shape have critical consequences for motility, immune system evasion, proliferation, and adhesion. For most bacteria, the peptidoglycan cell wall is both necessary and sufficient to determine cell shape. However, how the synthesis machinery assembles a peptidoglycan network with a robustly maintained micron-scale shape has remained elusive. To explore shape maintenance, we have quantified the robustness of cell shape in three Gram-negative bacteria in different genetic backgrounds and in the presence of an antibiotic that inhibits division. Building on previous modeling suggesting a prominent role for mechanical forces in shape regulation, we introduce a biophysical model for the growth dynamics of rod-shaped cells to investigate the roles of spatial regulation of peptidoglycan synthesis, glycan-strand biochemistry, and mechanical stretching during insertion. Our studies reveal that rod-shape maintenance requires insertion to be insensitive to fluctuations in cell-wall density and stress, and even a simple helical pattern of insertion is sufficient for over six-fold elongation without significant loss in shape. In addition, we demonstrate that both the length and prestretching of newly inserted strands regulate cell width. In sum, we show that simple physical rules can allow bacteria to achieve robust, shape-preserving cell-wall growth.

Keywords

bacterial cell shape; cell wall; peptidoglycan; growth; biophysics

Introduction

Bacteria control their shape with great precision and accuracy. Despite the enormous variety in bacterial morphology, cells of a particular species grown in a constant environment can maintain a characteristic shape through thousands of generations of growth(Philippe *et al.*, 2009). Many rod-shaped bacteria maintain a fixed direction and width as they elongate. Nevertheless, cells can adapt their shape and size in different osmotic environments or nutrient conditions, and cell size varies by 100-fold or more across the prokaryotic kingdom (Schulz, 2002, Bergey & Holt, 1994). Disregulation of cell shape has critical consequences for important functions such as motility (Mitchell, 2002), attachment (Rijnaarts *et al.*, 1995), and phagocytosis (Champion & Mitragotri, 2006), yet even for well-studied organisms such as the rod-shaped *Escherichia coli*, little is known about how shape and size are determined and maintained (Young, 2010).

*To whom correspondence should be addressed. Address: Department of Bioengineering, 318 Campus Drive West, Stanford University Stanford, CA 94305 USA, kchuang@stanford.edu, Phone: (650) 721-2483; Fax: (650) 724-1922.
†Current address: Biophysics Program, Harvard University, Cambridge, MA 02138.

The cell wall is both necessary and sufficient for determining cell shape (Yao *et al*., 1999, Holtje, 1998), and it plays a central mechanical role in cell integrity by bearing the stress generated by turgor pressures of several atmospheres (Boulbitch *et al.*, 2000). In both Gram-negative and Gram-positive bacteria, the cell wall is constructed of peptidoglycan, a polymer network composed of long, stiff glycan strands and flexible peptide crosslinks (Holtje, 1998). During cell growth, the peptidoglycan network must expand, and existing bonds must break in order for more material to be inserted into the network (Holtje & Heidrich, 2001). This process of breaking and inserting, however, can easily result in loss of a defined cell shape. What strategies and rules can bacteria employ in order to expand the peptidoglycan network while maintaining cell shape?

In previous work, we developed a quantitative mechanical model of the Gram-negative bacterial cell wall in which the glycan disaccharide subunits and peptide crosslinks are represented as stiff and flexible springs, respectively (Huang *et al.*, 2008). In our model, these springs form a single-layered network stretched by the outward force applied to the cytoplasmic membrane by turgor pressure (Gan *et al.*, 2008). For a given peptidoglycan spring network, the cell's shape is determined by the mechanical equilibrium. The parameters in our model are specified by experimental measurements of Young's modulus (Yao et al., 1999), of the persistence length of sugar strands (Cros *et al*., 1996), and of the 3D structure of the cell wall from cryo-electron tomography (Gan *et al.*, 2008).

We used our model to successfully predict the morphological response of *E. coli* cells to damage induced by vancomycin treatment. Our physical model also suggested that many common bacterial cell shapes could be realized via simple spatial patterning of the organization of peptidoglycan. In particular, we demonstrated that a helical pattern of modification to the crosslinking of a cylindrical peptidoglycan network causes relaxation into a helical shape, a mechanism which has since been shown to determine the shape of *Helicobacter pylori* (Sycuro *et al.*, 2010). Thus, our model provides a direct link between the static network structure of the cell wall and the shape that it imposes on the cell. Nevertheless, it remains an open question as to how such a network can be *grown* by the synthesis machinery. Here, we carry out simulations of rod-shaped Gram-negative cell walls during extensive insertion and crosslinking of new strands, and reveal that simple spatial patterns of the insertion machinery are sufficient to maintain rod shape while the biochemical and mechanical properties of the inserted strands dictate cell width.

Results

Experimental quantification of the width and shape of Gram-negative rod-shaped bacteria

To quantify the robustness of rod-shape maintenance in Gram-negative bacteria, we imaged thousands of wild-type *E. coli*, *Salmonella typhimurium*, and *Pseudomonas aeruginosa* cells and measured the variability of width, both along the length of individual cells and in the average width across the population. The average width of a population of 1340 wild-type *E. coli* K12 cells was 0.98±0.05 μm, and the width of the cylindrical portion of individual cells fluctuated by roughly 10%, both across the population (Fig. 1A) and within single cells (Fig. 1B). Moreover, the curves defining the cell midline could be fit to a straight line with an average R^2 value of 0.96, indicating that the cells grow as straight rods with a well-maintained width. Wild-type *S. typhimurium* LT2 and *P. aeruginosa* PA01 cells had slightly different widths from *E. coli* cells but also maintained shape and size (Fig. 1A). In contrast, a previously characterized CS612 mutant (Nelson & Young, 2000) lacking several genes in the peptidoglycan synthesis pathway (see Methods) exhibited dramatic variability in width across the population (1.42±0.23 μm, Fig. 1A), and width varied more within individual cells especially wider cells (Fig. 1C) and often failed to grow in a straight line. From these

experiments, it is clear that regulation of peptidoglycan synthesis is an important factor in the remarkable robustness of cell-shape determination in many Gram-negative bacteria.

Maintaining uniform insertion density preserves rod shape

Cell growth involves expansion of the cell wall, which requires a combination of breaking apart old material and inserting new strands. In spite of the potential for deformation after bond breakage due to the large turgor pressure, cells are able to elongate smoothly. It has been proposed that insertion of new material is tightly coordinated by a protein complex that colocalizes the hydrolysis of old material and the synthesis of new glycan strands (Koch, 1985). We modeled growth by selecting a crosslink for initiation of glycan synthesis, breaking peptide crosslinks along the path of insertion of a new strand, and crosslinking the new strand to the closest uncrosslinked old material (Fig. 2A, Methods). The cell wall relaxes to its lowest energy state between successive complete insertion events but not during insertion; this procedure mimics a ”make-before-break” scenario (Holtje, 1998). In simulations in which crosslinks were broken and the cell wall was relaxed prior to insertion, large pores were formed that were not closed by the following strand insertion event.

New strands were inserted with an average length of 20 disaccharide subunits approximately parallel to the existing strands, wrapping circumferentially around the longitudinal axis of the cell. The parameters in our model are based on experimental measurements when available, or reasonable assumptions otherwise (see Methods). Roughly N_g~1000 glycan subunits would be required to form a hoop with the circumference of an *E. coli* cell. Because computational expense rises proportional to both the length and circumference of the cell wall, most of our simulations were performed on cell walls starting with a circumference corresponding to N_g=100 glycan subunits. To compensate for this difference in cell size, we have scaled the peptide spring constant so that the network structure is insensitive to the value of N_g (see Methods).

We first assessed the consequences of random selection of initiation sites (Fig. 2B). If new material is inserted as complete hoops, the existing peptidoglycan serves as a sufficient template to maintain rod shape and width. However, new strands are typically much shorter than the circumference of the cell (Holtje, 1998), thus insertion unavoidably results in heterogeneity of peptidoglycan density. Using our *in silico* model with the site of insertion selected at random from among the peptide crosslinks between the two cell poles, we elongated a cell wall to six times its original length (Fig. 2C). The initial cell-wall network is composed of short glycan strands whose length distribution matches experimental measurements of *E. coli* MC4100 in LB (see Methods). Repeated strand insertion caused deviations from the initial rod shape (Fig. 2C), quickly causing bending and bulging at random sites along the cell wall. Because these sites had higher peptidoglycan density, the frequency of insertion at these points increased, resulting in a positive feedback that accentuated small deviations and led to rapid loss of rod shape and a large variation in width. By identifying the midline of the cell, we defined a local width, which varied by over 30% along the cell length.

To ascertain if elimination of the positive feedback between cell-wall density and insertion is sufficient to maintain rod shape, we modified our growth model so that insertion initiation sites were chosen with a uniform *density* (Fig. 2D). To do so, we assigned to each peptide crosslink a probability of selection that was inversely proportional to the local density of crosslinks, whereas in Fig. 2C that probability was constant. In contrast to Fig. 2B, cell walls grown using this uniform-insertion scheme maintained their rod shape through six-fold elongation (Fig. 2E). The local width was relatively constant at each elongation step, although the average width slowly increased as the cell wall elongated (Fig. 2F). We verified that the qualitative features of Figs. 2B–F did not depend on the set of stochastically

selected insertion sites; in over 100 independent simulations, the random insertion model produced severely deformed cells while the uniform-insertion model preserved rod shape. In *E. coli* (Varma *et al.*, 2007) and *Caulobacter crescentus* (Aaron et al., 2007), the cell-division protein FtsZ affects the localization of cell-wall synthesis. To incorporate FtsZ-mediated elongation, we modified our uniform-insertion scheme so that insertion was more probable near the poles and midcell and observed that rod-shape maintenance was unaffected (Fig. S1). Our results therefore suggest that uncoupling the spatial pattern of insertion from local variations in cell-wall density is sufficient for maintenance of cell shape.

Strand length and insertional stretching affect cell width

Wild-type *E. coli* cells treated with cephalexin cannot divide, and instead elongate to hundreds of microns in length. We measured the width of filamentous cells and found no increase in the average cell width, even for cells longer than 25 μm (Fig. 3D). We therefore examined whether the biophysical properties of the new strands could influence the cellular dimensions. First, biochemical changes to the insertion complexes could modify the average length L of new strands (Glauner *et al.*, 1988, Harz *et al.*, 1990). Second, mechanical forces could stretch the new strands as they are inserted (Koch & Doyle, 1985, Koch, 2001). If such insertional stretching occurs, the length of each glycan subunit will be greater than its relaxed length, resulting in new strands that require fewer subunits to span a given length (Fig. 3A, stretched purple strand composed of 7 subunits compared with 9 subunits in the unstretched blue strand).

As shown in Fig. 3B, we elongated cell walls to three times their original length using our uniform insertion model by systematically changing the preferred strand length and insertional stretching. The length of newly synthesized glycan strands is reduced by lytic transglycosylases (Glauner & Holtje, 1990); in our simulations, we assume that such cleavage has already taken place and strands have adopted a particular preferred length. We observed a consistent decrease in width as the length of inserted strands and the amount of insertional stretching was increased (Fig. 3C). We observed that pores in the cell wall were often larger near the ends of strands; hence inserting longer strands increased the overall average density of the peptidoglycan network. In addition, insertional stretching increased the density of crosslinking around the newly inserted strand. The width remained roughly constant for a number of combinations of strand length and insertional stretching (e.g., L=20, 10% stretching). We also elongated cells using our uniform insertion model with a Gaussian distribution of strand lengths length (20±5) to illustrate that the results are not sensitive to the precise length distribution (Fig. S2).

To verify that the cell wall reaches a steady-state width and network architecture, we simulated four rounds of elongation and division, starting from a single cell and producing 16 progeny. In each generation, the cell walls were elongated using the uniform insertion model in Fig. 2E–G until the amount of peptidoglycan doubled. The cell walls were then divided in half along a plane perpendicular to the longitudinal axis. We ignored the hemispherical poles since the mechanism of mechanical constriction during division is currently unclear, and instead stabilized the ends by appending seven complete glycan hoops at the beginning of each simulation. The first three generations of cells are shown in Fig. 4A, and the average cell width of the daughter cells is shown in Fig. 4B. The width was well maintained throughout the 16-fold increase in length, and several metrics of cell-wall organization converged toward steady-state values (Fig. S3). To establish that the average pore size would converge, we selected two cells from the fourth generation and verified convergence of cell width, average pore size, and pore-size distribution during three-fold elongation of these cells without division (Fig. S4). By contrast, in the random-insertion model neither strand length nor insertional stretching helped preserve cell shape or width

(Fig. S5). Taken together, our simulations suggest that while the spatial pattern of insertion controls the maintenance of cell shape, the molecular properties of the newly inserted strands control cell width.

Helical pattern of insertion sites maintains rod shape

We next explored other, more sparse spatial patterns that also uncouple insertion-site selection from the local cell-wall density. The actin homolog MreB forms filaments in *E. coli* (Wang *et al.*, 2010) that organize into helical patterns when overexpressed (Shih *et al.*, 2005). MreB also coordinates the localization of key components of the peptidoglycan synthesis machinery such as the transpeptidase PBP2 (Den Blaauwen *et al.*, 2003), and depolymerization of MreB by A22 treatment leads to progressive loss of rod shape (Shiomi *et al.*, 2008). We experimentally observed that *E. coli* cells initially continue to elongate when grown on an agarose pad with LB and A22 at 30 C, and adopted a lemon shape after several rounds of cell division (Supp. Movie 1). Moreover, cells grown on an agarose pad with LB, A22, and cephalexin at 30 C after 30 minutes of liquid growth in LB and cephalexin did not adopt a lemon-shaped morphology; instead, the cells filamented but lost their ability to maintain cell width, with morphologies reminiscent of the local self-similar growth results in Fig. 2C (Fig. 5D, Supp. Movies 2 and 3).

To address one possible mechanism of MreB-mediated insertion, we modified our uniform insertion model so that potential insertion sites were chosen only if they lay near a fixed helix positioned interior to the cell wall and extending the length of the cell (Fig. 5A). We found that with a helical pitch angle from 0.5 to 18 degrees, this parsimonious pattern of insertion preserves rod shape (Fig. 5B) and cell width (Fig. 5C), with similar efficacy as the uniform insertion model in Fig. 2E–G. As the cell wall elongated, newly inserted strands ended up migrating away from the fixed helix in a roughly circumferential direction due to subsequent insertion events. The inserted material (blue strands in Fig. 5B) ended up evenly distributed across the cylindrical surface, thereby avoiding the positive feedback that causes bending and bulging for random insertion (Fig. 2C) and suggesting that helical structures such as MreB may provide a biological mechanism for achieving the homogeneous insertion of cell-wall material necessary for maintaining a rod shape.

Recent single-molecule experiments have suggested that MreB may form short, treadmilling filaments (Kim *et al.*, 2006). To test whether fragmentation or movement of the MreB helix would affect rod-shaped maintenance, we performed simulations in which the MreB helix was split up into four segments each with a fixed pitch angle of 18 degrees. The MreB segments were randomly oriented about the circumference relative to one another, and their orientation was reset randomly, as if spinning them about the longitudinal axis of the cell, on a time scale corresponding to ~25% of the cell cycle. This growth model was also sufficient to maintain rod shape (Fig. S6), indicating that cell-shape maintenance from a helical pattern is not sensitive to the fragmentation or movement of the molecular structures defining the helix. Intriguingly, we observe that if the pitch angle becomes too large, rod-shaped growth is not maintained (Fig. S7), due to an obvious increase in cell-wall density near the helical insertion zones. These data suggest that the spatial pattern of insertion need not extend across the entire cell surface, as long as insertion remains uncoupled from cell-wall density.

A22-treatment causes growth into a round morphology in *E. coli* (Varma et al., 2007), *C. crescentus* (Cowles & Gitai, 2010), and *P. aeruginosa* (Cowles & Gitai, 2010), leading to the hypothesis that the default mode of growth in the absence of MreB is spherical. However, at least two rounds of cell division are required before the loss of rod-shape is apparent (Fig. 6A, Supp. Movie 1). Moreover, in *C. crescentus*, elongation is also affected by the FtsZ-dependent midcell recruitment of MurG, the enzyme responsible for synthesis of the essential peptidoglycan precursor lipid II (Aaron et al., 2007); a similar FtsZ-dependent

elongation is observed in *E. coli* as well. Therefore, we speculated that cells would continue to elongate in the absence of both MreB and FtsZ, and that such growth would resemble the random insertion model of elongation in Fig. 2C. After treating *E. coli* K12 cells with cephalexin for 60 minutes to ensure that division was inhibited, we observed the subsequent growth on agarose pads with 10 μg/ml A22. Most cells continued to elongate into filaments (Fig. 6B), and cell width became significantly more variable (Fig. 6C), in a manner similar to our simulations using random insertion (Fig. 2C). Furthermore, cell growth eventually led to the formation of a bulge whose rapid growth signaled the demise of the cell. Previous experiments inhibiting both FtsZ and MreB using SulA expression and A22-treatment (2μg/ml) in an *E. coli* mutant lacking PBP5 and PBP7 also demonstrated that cells would elongate with a variable width (Varma et al., 2007). At higher A22 levels (5μg/ml), cells swelled in the middle to a large width and retained cylindrical endcaps. This difference in morphology may be due either to the absence of PBPs 5 and 7 or to the method of FtsZ inhibition (expression of SulA from a plasmid). Regardless, our results suggest that elongation in the absence of MreB and FtsZ occurs via random insertion of glycan strands, which reduces the cell's ability to maintain its rod shape and integrity.

Tension-dependent insertion does not maintain cell shape

Our model can also reveal the inability of a potential insertion scheme to maintain cell shape. For example, we can directly test whether insertion in a tension-sensitive manner can stabilize the bending and bulging due to random self-similar insertion (Cabeen *et al.*, 2009). In practice, we choose the starting peptide with a probability that increases exponentially with the spring extension energy $k_p \Delta x_p^2/2$ (see Methods). We found that the regions under the largest stress were the peptides surrounding newly inserted strands (Fig. 7A,B), a somewhat counterintuitive observation given that one might naively expect a newly inserted strand to relax the tension locally. However, there was typically a mismatch in the circumferential alignment of the vertices on the new strand with the nearby vertices in the surrounding network that caused the new crosslinks to be more stretched than the old crosslinks. Therefore, we observed that sites of insertion were highly biased toward the material surrounding recent insertion events, again leading to a positive feedback in insertion that caused rapid loss of cell shape (Fig. 7C). This suggests that the peptidoglycan synthesis machinery is likely not specifically targeted to regions of high stress.

Discussion

Despite extensive characterization of the biochemical properties and genetic determinants of the bacterial cell wall, fundamental physical questions about how bacteria maintain their shape and size remain unanswered. To investigate cell-shape maintenance in rod-shaped Gram-negative bacteria, we developed a biophysical model for simulating growth dynamics, allowing for different mechanisms of insertion of new cell-wall material. Using this model, we examined the three main factors dictating the insertion of new glycan strands: (*i*) geometry, via the spatial patterning of new material, (*ii*) biochemistry, via the likelihood of strand termination, which dictates average inserted strand length, and (*iii*) mechanics, via forces exerted by the insertion machinery on new strands. Through a quantitative, multi-dimensional exploration of these three factors, we found that maintenance of cell shape depends on uncoupling the spatial pattern of insertion from the local cell-wall density, while determination of cell width depends on a combination of the average length and the mechanical stretching of new strands during insertion. Moreover, our model can also be used to reveal the failure of qualitative models such as tension-dependent insertion (Fig. 7) to maintain cell shape.

Rod-shaped bacteria such as *E. coli*, *S. typhimurium*, and *P. aeruginosa* robustly maintain a cylindrical shape during exponential growth (Fig. 1). Thus, while each species has its own well-defined radius, the precise maintenance of cell shape is likely general across species. Although we have focused primarily on experiments involving *E. coli*, our modeling is intended to test general principles of cell growth, rather than the consequences of particular parameters. Moreover, many parameters such as the Young's modulus may in fact be similar even across evolutionarily distant organisms. For example, despite significant differences between the peptidoglycan architectures of *E. coli* and the Gram-positive *Bacillus subtilis*, atomic-force microscopy measurements indicate that both species have a Young's modulus of ~25 MPa (Yao et al., 1999, Thwaites & Surana, 1991). In any event, we hope that our computational framework will motivate further experimental measurements of the biophysical properties and organization of peptidoglycan across a range of species.

Intriguingly, *E. coli* can revert to a straight morphology even after large morphological perturbations. *E. coli* spheroplasts slowly revert back to a rod shape after lysozyme is removed as the cell wall regrows over multiple generations (Schwarz & Leutgeb, 1971). Filamentous *E. coli* cells grown in circular agarose microchambers have a curved morphology determined by the chamber geometry, but grow into an increasingly straight conformation when released from the chamber (Takeuchi *et al.*, 2005). It has been hypothesized that in order for this growth-dependent straightening to occur, insertion of new peptidoglycan cannot depend only on local self-similar growth, instead there must be a global structure coordinating the insertion of new material (Sliusarenko *et al.*, 2010, Mukhopadhyay & Wingreen, 2009). Our simulations also conclude that robust rod-shaped cell-wall growth can be achieved by inserting new material with constant longitudinal and azimuthal density, uncoupled from local peptidoglycan density. We also demonstrated that self-similar growth initiated from random locations along the cell wall results in cell-wall density fluctuations that grow due to positive feedback. Starting from a straight cell, these model cell walls exhibited noticeable departures from a straight morphology after less than one doubling. At later stages of growth, cells were severely bent and bulged outwards with a variation in local width of ~50%. Our results indicate that cell-wall synthesis must be regulated in order to maintain shape, and that spatial control alone is sufficient.

Using our model, we also explored the consequences of peptidoglycan insertion in a fixed helical pattern or along a pattern of short helical segments, both of which are much sparser patterns than uniform insertion in which only a tiny percentage (<1%) of the peptide crosslinks are viable initiation sites at any one time (Fig. 2E–G). We found that rod shape was preserved with similar fidelity to completely uniform insertion. Newly inserted material was shifted progressively farther away from insertion helix by subsequent insertion events, resulting in a flow of new material that homogenized the distribution of insertion. These results suggest that insertion patterns such as patches and short filaments may also be effective at maintaining a rod shape as long as the resulting pattern of inserted material becomes uniform after sufficient growth. Indeed, rod shape was also maintained when the fixed helical pattern was replaced by four dynamic helical segments covering the length of the cell whose angular orientations were independently and randomly selected every time the cell length increased by 33% (Fig. S6).

Most rod-shaped bacteria contain cytoskeletal proteins thought to form global structures within the cell. The actin homolog MreB forms filaments (Wang et al., 2010) that organize into helical patterns when overexpressed (Shih et al., 2005). MreB also coordinates the localization of key components of the peptidoglycan synthesis machinery such as the transpeptidase PBP2 (Den Blaauwen et al., 2003), and the flexural rigidity of *E. coli* cells drops by 50% under A22-treatment that depolymerizes MreB (Wang et al., 2010), suggesting that the MreB structure and the cell wall make comparable contributions to cell

stiffness. The stiffness of the MreB structure and its localization on the cytoplasmic face of the inner membrane may enable the spatial organization of peptidoglycan insertion to be independent of the existing cell-wall density. *E. coli* and *C. crescentus* cells treated with A22 initially maintain a rod shape but eventually grow into lemon-shaped morphologies (Supp. Movie 1) (Varma *et al.*, 2007, Gitai *et al.*, 2005). Moreover, *E. coli* cells treated with both cephalexin and A22 continue to elongate but have variable width and eventually lyse due to bulging of the cytoplasmic membrane through large pores in the cell wall (Fig. 6, Supp. Movies 2 and 3). Similarly, in our simulations cell walls growing via random insertion initially remain straight, and only lose rod shape later in growth as cell-wall disorganization increases. Taken together, these results suggest a specific role for the MreB cytoskeleton in rod-shape maintenance, namely use of the structural rigidity of MreB to decouple insertion of new strands from local peptidoglycan density.

In addition to maintaining a specific shape, many rod-shaped Gram-negative bacteria faithfully maintain a specific width dependent on species and growth conditions (Fig. 1). By individually varying the biochemical and mechanical characteristics of newly inserted strands, we have elucidated an interplay between strand termination and insertional stretching that would allow cells to modulate their width. In particular, changes in cell width depend inversely on two factors: (*i*) the average strand length, which scales inversely with the termination probability during strand synthesis, and (*ii*) the stretching force exerted by the insertion complex on new strands as they are crosslinked to the existing network. Differences in the distribution of glycan strands have been experimentally measured across morphological variants of cells of a single species and across cells of different species. *E. coli* cells grown in LB in stationary phase are more spherical and have an average glycan strand length of 17.8 disaccharides, whereas *E. coli* grown in PB at 42°C have an average strand length of 37.9 (Glauner *et al.*, 1988). Round *E. coli* minicells, formed by polar divisions, have shorter strands and altered concentrations of penicillin binding proteins (Obermann & Holtje, 1994). Moreover, peptidoglycan glycosyltransferases from different bacterial species produce different glycan chain lengths *in vitro* (Wang *et al.*, 2008). Thus, our modeling suggests that *E. coli* cells can alter their width by varying the processivity of strand synthesis, a prediction that could be tested via measurement of the strand length distribution before and after cells are shifted from a low-nutrient medium (e.g., M9-glucose, in which cell width is ~0.6 μm) to a rich medium (e.g., LB, in which width is ~1 μm).

Insertional stretching has been hypothesized as a width-maintenance mechanism in a previous theoretical study that used a continuum model of cell-wall mechanics to argue that the undeformed radius of the newly added material must be less than the current cell radius in order to accommodate pressure-mediated expansion (Lan *et al.*, 2007). Our studies reveal that roughly 10% stretching is required to maintain a fixed width, and show that increased stretching is correlated with an increase in the fraction of crosslinked glycans and an increase in the rigidity of the cell wall near sites of recent insertion, both of which could serve as experimental signatures of insertional stretching. This degree of insertional stretching would require ~5–10 pN of force per glycan subunit, which could be provided by the chemical energy released by crosslinking of the new strand to the old network (Jiang & Sun, 2010) or by the insertion machinery during synthesis (Holtje, 1998). Insertion complexes may also perform a dual mechanical function by exerting forces on newly inserted strands and restraining the expansion of the existing material during hydrolysis to maximize crosslinking potential. Based on our computational result that the cell wall reaches a steady-state level of organization after sufficient elongation using a given growth model (Fig. S3) and our experimental observation that the width of filamentous *E. coli* is identical to wild-type cells, we predict that the glycan strand length distribution in the cylindrical portion of the cell wall is largely unaffected by cephalexin treatment. Taken together, our results suggest that differences in strand length distributions and crosslinking density

contribute to differences in cell width. Our computational framework can be used to investigate the rules governing shape determination and the strategies a cell might employ to grow its cell wall in a robust manner.

Our modeling of cell-wall growth reinforce the principle that systematic spatial variation of insertion probability could lead to variant rod shapes such as curved or helical cells. Moreover, our simulations of helical growth predict that old cell-wall material will move apart in a specific pattern that could be observed by pulse-chase labeling of peptidoglycan. Both our computational (Fig. 2C) and experimental results (Fig. 6) predict that in the absence of a global MreB-mediated template for insertion, the loss of rod-shape maintenance is coupled to the formation of large pores that could be measurable via cryo-electron tomography (Gan et al., 2008) or AFM (Hayhurst *et al.*, 2008). In the future, incorporating external and cytoskeletal forces into our models will enable the study of peptidoglycan organization for cells growing in confined geometries (Takeuchi et al., 2005), curved species such as *C. crescentus* (Cabeen et al., 2009), and morphological transitions such as cell division (Osawa *et al.*, 2008).

Because the biochemical properties of peptidoglycan are highly conserved across prokaryotes, our results have elucidated mechanisms that may have broad applicability across even highly divergent species. Indeed, homologs to the *pbp2* and *mreB* genes are found in a large fraction of rod-shaped bacteria, and the small-molecule inhibitor A22 has similar impact on cell shape in all species with MreB. Thus, simulations provide an effective tool for assigning morphological consequences to each of the molecular properties of the peptidoglycan synthesis machinery, and for testing the effectiveness of different mechanisms of cell growth. In the future, expanding this study to include bacterial species of a variety of shapes and sizes could reveal general mechanisms for manipulating and controlling bacterial growth and division.

Methods

Bacterial growth conditions

Experiments were performed on the wild-type strains *E. coli* K12, *S. typhimurium* LT2, and *P. aeruoginosa* PA01, and the previously described CS612 *mrcA dacB dacA dacC pbpG ampC ampH E. coli* strain (Nelson & Young, 2000). Cells used for imaging were grown to log phase (OD_{600}= 0.5–0.8) in LB. Unless otherwise noted, cells were grown at 37 C. Cephalexin was used at a concentration of 25 μg/ml. A22 was used at a concentration of 10 μg/ml. Live-cell imaging experiments were performed by pipetting exponentially growing cells onto a 1% agarose pad. All images were captured with a Nikon Ti-E microscope and a DU-885 cooled CCD camera (Andor) using μManager software. Cell shape was analyzed using PSICIC (Guberman *et al.*, 2008). The cylindrical portion of the cell was determined by fitting the width profile to a cylinder with hemispherical endcaps, and the variability in cell width was determined from the subset of 200 points along the perimeter corresponding to the cylinder.

Biophysical model for peptidoglycan mechanics

Our model for the organization of Gram-negative peptidoglycan is discussed in detail in (Huang *et al.*, 2008). In brief, we treat the cell wall as a single-layer network of springs. A maximally connected rod-shaped cell wall is constructed from N_h hoops of N_g glycans each, connected by peptide crosslinks. Each vertex lies at the end of two glycans and one peptide. Endcaps were created by adding hoops to the ends of the cell wall with a decreasing numbers of glycans selected to produce a hemispherical shape. The cell walls that serve as

starting points for our simulations are created by randomly removing peptides and glycans so that the experimentally measured glycan strand length distribution is reproduced.

The equilibrium state of a network is determined by minimizing the sum of energetic contributions from spring extension, glycan bending, and turgor pressure. Glycans and peptides are represented as Hookean springs. The peptide spring constant k_p=10 pN/nm has been estimated from AFM measurements of the Young's modulus of *E. coli* sacculi (25 MPa (Yao et al., 1999)). The glycan spring constant k_g=50 pN/nm is taken to be larger than the peptide spring constant to reflect the stiffness of the glycan strands relative to the peptide crosslinks; for this value of k_g there is little stretching in the glycans (Fig. S3G), hence further increase in k_g has virtually no effect. The relaxed lengths d_g=2 nm and d_p=1 nm were estimated from NMR structural studies (Meroueh *et al.*, 2006). Bending energies are evaluated for glycan-glycan orientations at an angle θ using $E_{\text{bend}}(\theta) = \alpha(\theta - \pi)^6/6$ with α =0.1, which penalizes large kinking angles between glycans while allowing small deviations of θ from π. The value α was estimated from experimental measurements of the persistence lengths of pectin polysaccharids (~10nm (Cros et al., 1996)). The turgor pressure of *E. coli* cells varies from ~0.5 to 3 atm depending on growth media osmolality (Cayley *et al.*, 2000). We have assumed an intermediate value of P=1 atm although we note that our qualitative observations hold over a large range of turgor pressures. The turgor-pressure energy is the product of the turgor pressure and the cell volume. The volume of the cell is determined by evaluating the surface integral of the function $f(x,y,z)=x$ over each face of the polyhedron. The faces of the polyhedron are initially determined geometrically and subsequently updated during insertion events using a shortest-cycle algorithm (Bagali & Warren N. Waggenspack, 1995). The energy is minimized using a nonlinear conjugate gradient algorithm, and all simulations were performed using custom C++ code.

Computational expense rises proportional to both the length and circumference of the cell wall, and the need for growth simulations to be tractable currently limits our study to cell walls smaller than typical *E. coli* cells, for which roughly N_g~1000 glycan subunits would be required to surround the circumference (Boulbitch et al., 2000). Most simulations were performed on cell walls starting with an average circumference corresponding to the length of a hoop with N_g=100 glycan subunits. The width of the cell is ~$N_g d_g/\pi$, thus the cross-sectional area $A \propto N_g^2 d_g^2$. The outward force exerted on the endcaps is PA, resulting in a restoring force $k_p N_g \Delta x_p/2$ borne by the peptide crosslinks. Therefore, the extension in each peptide $\Delta x_p \sim P d_g^2 N_g/k_p$ scales linearly with N_g. To recapitulate the energy balance between spring stretching and turgor pressure found in micron-sized *E. coli* cells, we rescale k_p. Since we are interested in the dynamics of the network structure during growth, we scale k_p proportional to N_g to keep Δx_p and the pore size distribution approximately constant. Given that for an *E. coli* sacculus k_p~10 pN/nm and N_g~1000, we set k_p=1 pN/nm for our model cell walls with N_g=100. We have also verified that after scaling k_p with N_g, growth simulations with larger hoops (e.g., N_g=200) give similar results.

Cell-wall growth

We model growth by selecting a peptide crosslink for initiation of glycan synthesis, breaking peptide crosslinks along the path of insertion of a new strand, and crosslinking the new strand to the closest uncrosslinked old material (Fig. 2A). New strands are inserted approximately parallel to the existing strands, wrapping circumferentially around the longitudinal axis of the cell.

The starting peptide crosslink in each insertion is chosen in different ways. In the random insertion scheme, the starting peptide is the closest peptide to a randomly chosen point on the cell surface. In the uniform insertion scheme, the starting peptide is chosen randomly with a uniform azimuthal and longitudinal density. In the helical insertion scheme, the

starting peptide is chosen randomly along a fixed helical pattern. In the tension-dependent insertion scheme, the starting peptide is chosen with a probability proportional to a Boltzmann factor $e^{E/\tau}$, where E is the Hookean spring energy of each spring, and τ is a temperature, taken here to be 0.5 pN nm.

After the starting peptide is chosen, peptides are removed from adjacent glycan strands along a path in the circumferential direction until the free path exceeds a defined length L. Since only peptides in adjacent polygons are removed, planarity is maintained. If the local geometry requires the strand to deviate too far from the circumferential direction, removal of peptides stops even if the free path has not reached L. Once the glycan strand has been created, it is subdivided into glycan subunits of length d_g, or in the case of insertional stretching, of length $\sigma\, d_g$, where σ is the stretching parameter. In all cases, the new glycans have stiffness k_g. Peptides along the glycan strand cross-link to the closest in-plane free peptide in the old material, within a radius of 5 nm. Large pores tend to be created near the ends of newly inserted strands, mostly due to the geometry since a previously existing crosslink is replaced with a new crosslink that connects the end of the new strand only to one side of the old crosslink.

Center-line identification

Given a cell with N_v vertices, we consider a fictitious chain of n_c springs and minimize their positions subject to the energy functional

$$E_{center}=\sum_{i=1}^{n_c}\frac{k_s}{n_c}(l_i-l_0)^2+\sum_{i=1}^{n_i}\frac{k_\theta}{n_c}(\theta_s-\theta_0)^2+\sum_{j=1}^{N_v}\frac{k_v}{N_v}\left(\delta_j-\delta_0\right)^2 \quad (1)$$

where l_i are the lengths of the springs in the chain, θ_i are the angles between springs, and θ_j is the minimum distance of each vertex to the chain. For cells with N_g=100, we took n_c=30, k_s=0.005, l_0=10, k_θ =1000, $\theta_0 = \pi$, k_v=0.001, and δ_0=40. The local width is then determined as the shortest distance to the center line.

Supplementary Material

Refer to Web version on PubMed Central for supplementary material.

Acknowledgments

The authors would like to thank members of the Huang lab, Chris Henley, Joshua Shaevitz, and Steven Wang for useful discussions, and Kevin Young for the CS612 strain. This work was funded in part by NIH grants K25 GM075000 and the NIH Director's New Innovator Award DP2OD006466 to K.C.H. and NIH grant number R01 GM073186 to N.S.W.

Bibliography

Aaron M, Charbon G, Lam H, Schwarz H, Vollmer W, Jacobs-Wagner C. The tubulin homologue FtsZ contributes to cell elongation by guiding cell wall precursor synthesis in Caulobacter crescentus. Mol Microbiol. 2007; 64:938–952. [PubMed: 17501919]

Bagali, S.; Warren, J.; Waggenspack, N. A shortest path approach to wireframe to solid model conversion; Proceedings of the third ACM symposium on Solid modeling and applications; Salt Lake City, Utah, United States: ACM; 1995. p. 339-350.

Bergey, DH.; Holt, JG. Bergey's manual of determinative bacteriology. Baltimore: Williams & Wilkins; 1994. p. xviii-787.

Boulbitch A, Quinn B, Pink D. Elasticity of the rod-shaped gram-negative eubacteria. Phys Rev Lett. 2000; 85:5246–5249. [PubMed: 11102232]

Cabeen MT, Charbon G, Vollmer W, Born P, Ausmees N, Weibel DB, Jacobs-Wagner C. Bacterial cell curvature through mechanical control of cell growth. EMBO J. 2009; 28:1208–1219. [PubMed: 19279668]

Cayley DS, Guttman HJ, Record MT Jr. Biophysical characterization of changes in amounts and activity of Escherichia coli cell and compartment water and turgor pressure in response to osmotic stress. Biophys J. 2000; 78:1748–1764. [PubMed: 10733957]

Champion JA, Mitragotri S. Role of target geometry in phagocytosis. Proc Natl Acad Sci U S A. 2006; 103:4930–4934. [PubMed: 16549762]

Cowles KN, Gitai Z. Surface association and the MreB cytoskeleton regulate pilus production, localization and function in Pseudomonas aeruginosa. Mol Microbiol. 2010; 76:1411–1426. [PubMed: 20398206]

Cros S, Garnier C, Axelos MA, Imberty A, Perez S. Solution conformations of pectin polysaccharides: determination of chain characteristics by small angle neutron scattering, viscometry, and molecular modeling. Biopolymers. 1996; 39:339–352. [PubMed: 8756514]

Den Blaauwen T, Aarsman ME, Vischer NO, Nanninga N. Penicillin-binding protein PBP2 of Escherichia coli localizes preferentially in the lateral wall and at mid-cell in comparison with the old cell pole. Mol Microbiol. 2003; 47:539–547. [PubMed: 12519203]

Gan L, Chen S, Jensen GJ. Molecular organization of Gram-negative peptidoglycan. Proc Natl Acad Sci U S A. 2008; 105:18953–18957. [PubMed: 19033194]

Gitai Z, Dye NA, Reisenauer A, Wachi M, Shapiro L. MreB actin-mediated segregation of a specific region of a bacterial chromosome. Cell. 2005; 120:329–341. [PubMed: 15707892]

Glauner B, Holtje JV. Growth pattern of the murein sacculus of Escherichia coli. J Biol Chem. 1990; 265:18988–18996. [PubMed: 2229056]

Glauner B, Holtje JV, Schwarz U. The composition of the murein of Escherichia coli. J Biol Chem. 1988; 263:10088–10095. [PubMed: 3292521]

Guberman JM, Fay A, Dworkin J, Wingreen NS, Gitai Z. PSICIC: noise and asymmetry in bacterial division revealed by computational image analysis at sub-pixel resolution. PLoS Comput Biol. 2008; 4:e1000233. [PubMed: 19043544]

Harz H, Burgdorf K, Holtje JV. Isolation and separation of the glycan strands from murein of Escherichia coli by reversed-phase high-performance liquid chromatography. Anal Biochem. 1990; 190:120–128. [PubMed: 2285138]

Hayhurst EJ, Kailas L, Hobbs JK, Foster SJ. Cell wall peptidoglycan architecture in Bacillus subtilis. Proc Natl Acad Sci U S A. 2008; 105:14603–14608. [PubMed: 18784364]

Holtje JV. Growth of the stress-bearing and shape-maintaining murein sacculus of Escherichia coli. Microbiol Mol Biol Rev. 1998; 62:181–203. [PubMed: 9529891]

Holtje JV, Heidrich C. Enzymology of elongation and constriction of the murein sacculus of Escherichia coli. Biochimie. 2001; 83:103–108. [PubMed: 11254982]

Huang KC, Mukhopadhyay R, Wen B, Gitai Z, Wingreen NS. Cell shape and cell-wall organization in Gram-negative bacteria. Proc Natl Acad Sci U S A. 2008; 105:19282–19287. [PubMed: 19050072]

Jiang H, Sun SX. Morphology, growth, and size limit of bacterial cells. Phys Rev Lett. 2010; 105:028101. [PubMed: 20867742]

Kim SY, Gitai Z, Kinkhabwala A, Shapiro L, Moerner WE. Single molecules of the bacterial actin MreB undergo directed treadmilling motion in Caulobacter crescentus. Proc Natl Acad Sci U S A. 2006; 103:10929–10934. [PubMed: 16829583]

Koch AL. How bacteria grow and divide in spite of internal hydrostatic pressure. Can J Microbiol. 1985; 31:1071–1084. [PubMed: 3938340]

Koch, AL. Bacterial growth and form. Boston: Kluwer Academic Publishers, Dordrecht; 2001. p. 470

Koch AL, Doyle RJ. Inside-to-outside growth and turnover of the wall of gram-positive rods. J Theor Biol. 1985; 117:137–157. [PubMed: 3935878]

Lan G, Wolgemuth CW, Sun SX. Z-ring force and cell shape during division in rod-like bacteria. Proc Natl Acad Sci U S A. 2007; 104:16110–16115. [PubMed: 17913889]

Meroueh SO, Bencze KZ, Hesek D, Lee M, Fisher JF, Stemmler TL, Mobashery S. Three-dimensional structure of the bacterial cell wall peptidoglycan. Proc Natl Acad Sci U S A. 2006; 103:4404–4409. [PubMed: 16537437]

Mitchell JG. The energetics and scaling of search strategies in bacteria. Am Nat. 2002; 160:727–740. [PubMed: 18707461]

Mukhopadhyay R, Wingreen NS. Curvature and shape determination of growing bacteria. Phys Rev E Stat Nonlin Soft Matter Phys. 2009; 80:062901. [PubMed: 20365209]

Nelson DE, Young KD. Penicillin binding protein 5 affects cell diameter, contour, and morphology of Escherichia coli. J Bacteriol. 2000; 182:1714–1721. [PubMed: 10692378]

Obermann W, Holtje JV. Alterations of murein structure and of penicillin-binding proteins in minicells from Escherichia coli. Microbiology. 1994; 140(Pt 1):79–87. [PubMed: 8162193]

Osawa M, Anderson DE, Erickson HP. Reconstitution of contractile FtsZ rings in liposomes. Science. 2008; 320:792–794. [PubMed: 18420899]

Philippe N, Pelosi L, Lenski RE, Schneider D. Evolution of penicillin-binding protein 2 concentration and cell shape during a long-term experiment with Escherichia coli. J Bacteriol. 2009; 191:909–921. [PubMed: 19047356]

Rijnaarts HHM, Norde W, Bouwer EJ, Lyklema J, Zehnder AJB. Reversibility and mechanism of bacterial adhesion. Colloids and Surfaces B: Biointerfaces. 1995; 4:5–22.

Schulz HN. Thiomargarita namibiensis: Giant microbe holding its breath. Asm News. 2002; 68 122-+

Schwarz U, Leutgeb W. Morphogenetic aspects of murein structure and biosynthesis. J Bacteriol. 1971; 106:588–595. [PubMed: 4929868]

Shih YL, Kawagishi I, Rothfield L. The MreB and Min cytoskeletal-like systems play independent roles in prokaryotic polar differentiation. Mol Microbiol. 2005; 58:917–928. [PubMed: 16262780]

Shiomi D, Sakai M, Niki H. Determination of bacterial rod shape by a novel cytoskeletal membrane protein. EMBO J. 2008; 27:3081–3091. [PubMed: 19008860]

Sliusarenko O, Cabeen MT, Wolgemuth CW, Jacobs-Wagner C, Emonet T. Processivity of peptidoglycan synthesis provides a built-in mechanism for the robustness of straight-rod cell morphology. Proc Natl Acad Sci U S A. 2010; 107:10086–10091. [PubMed: 20479277]

Sycuro LK, Pincus Z, Gutierrez KD, Biboy J, Stern CA, Vollmer W, Salama NR. Peptidoglycan crosslinking relaxation promotes Helicobacter pylori's helical shape and stomach colonization. Cell. 2010; 141:822–833. [PubMed: 20510929]

Takeuchi S, DiLuzio WR, Weibel DB, Whitesides GM. Controlling the shape of filamentous cells of Escherichia coli. Nano Lett. 2005; 5:1819–1823. [PubMed: 16159230]

Thwaites JJ, Surana UC. Mechanical properties of Bacillus subtilis cell walls: effects of removing residual culture medium. J Bacteriol. 1991; 173:197–203. [PubMed: 1898920]

Varma A, de Pedro MA, Young KD. FtsZ directs a second mode of peptidoglycan synthesis in Escherichia coli. J Bacteriol. 2007; 189:5692–5704. [PubMed: 17513471]

Wang S, Arellano-Santoyo H, Combs PA, Shaevitz JW. Actin-like cytoskeleton filaments contribute to cell mechanics in bacteria. Proc Natl Acad Sci U S A. 2010; 107:9182–9185. [PubMed: 20439764]

Wang TS, Manning SA, Walker S, Kahne D. Isolated peptidoglycan glycosyltransferases from different organisms produce different glycan chain lengths. J Am Chem Soc. 2008; 130:14068–14069. [PubMed: 18834124]

Yao X, Jericho M, Pink D, Beveridge T. Thickness and elasticity of gram-negative murein sacculi measured by atomic force microscopy. J Bacteriol. 1999; 181:6865–6875. [PubMed: 10559150]

Young KD. Bacterial shape: two-dimensional questions and possibilities. Annu Rev Microbiol. 2010; 64:223–240. [PubMed: 20825347]

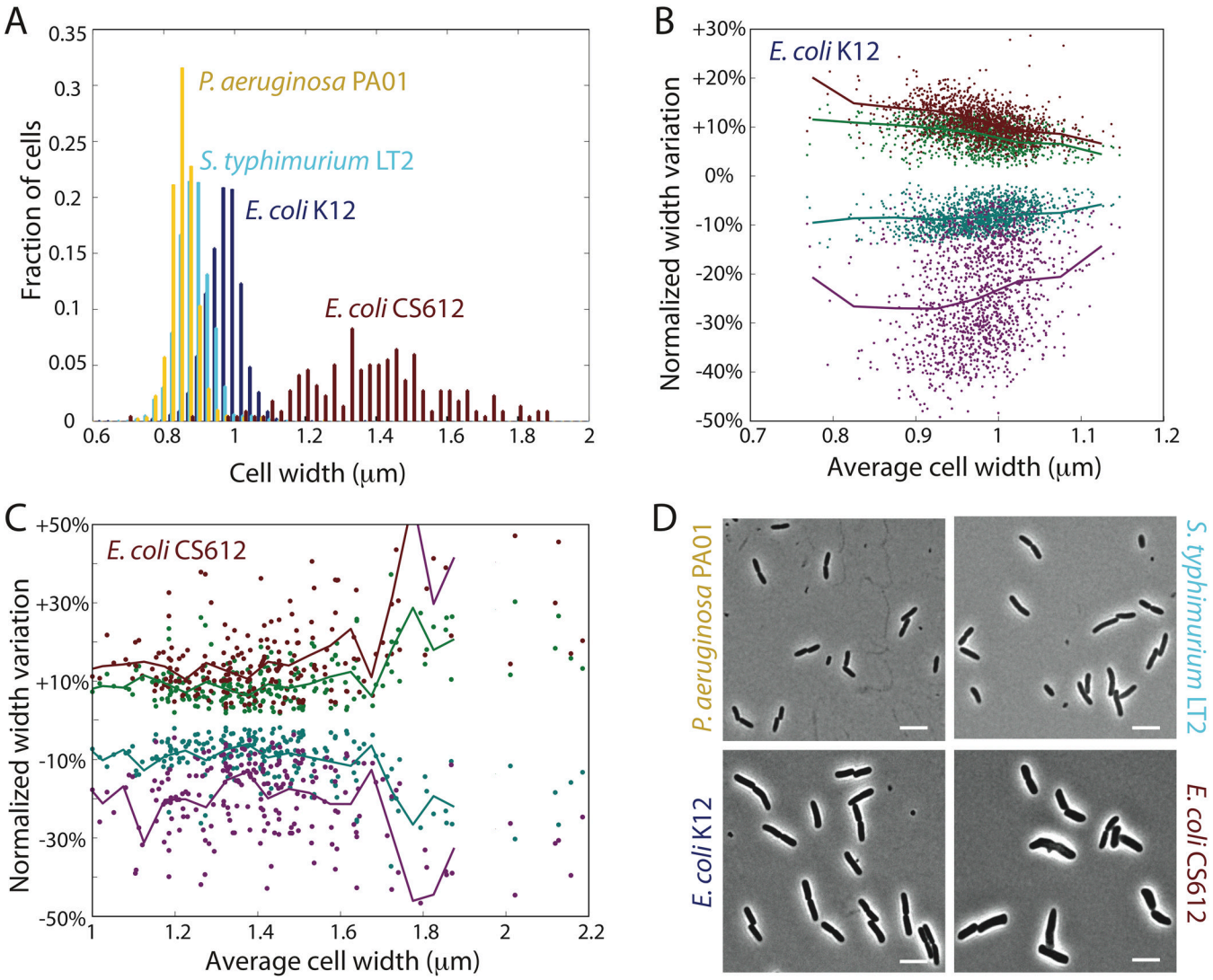

Figure 1. Cell width is tightly controlled in rod-shaped Gram-negative bacteria

(A) Distributions of cell widths: average cell width across a population of 1340 wild-type *E. coli* K12 cells is 0.98±0.05 μm. Similar width maintenance occurs in *S. typhimurium* LT2 (0.89±0.05 μm, 960 cells) and *P. aeruginosa* PA01 (0.86±0.04 μm, 785 cells). Multiple PBP-deletion strain *E. coli* CS612 has a much broader distribution of widths (1.42±0.23 μm, 217 cells). (B) Intracellular width variation: for each of the 1340 *E. coli* K12 cells in A, we calculated the standard deviation of the width across each cell, as well as the minimum and maximum width within each cell (discounting the poles). Each green/teal circle corresponds to plus/minus one standard deviation normalized by the average width of a single cell. Each red/purple circle corresponds to the maximum/minimum width normalized by the average width. Solid lines are averages over cells grouped in bins of size 0.05 μm according to their average width. The width variability within cells remains roughly constant for different average widths (~10%). (C) Similar to B, measures of intracellular width variability in *E. coli* CS612 cells. (D) Representative phase-contrast micrographs for each strain. Scale bars are 5 μm.

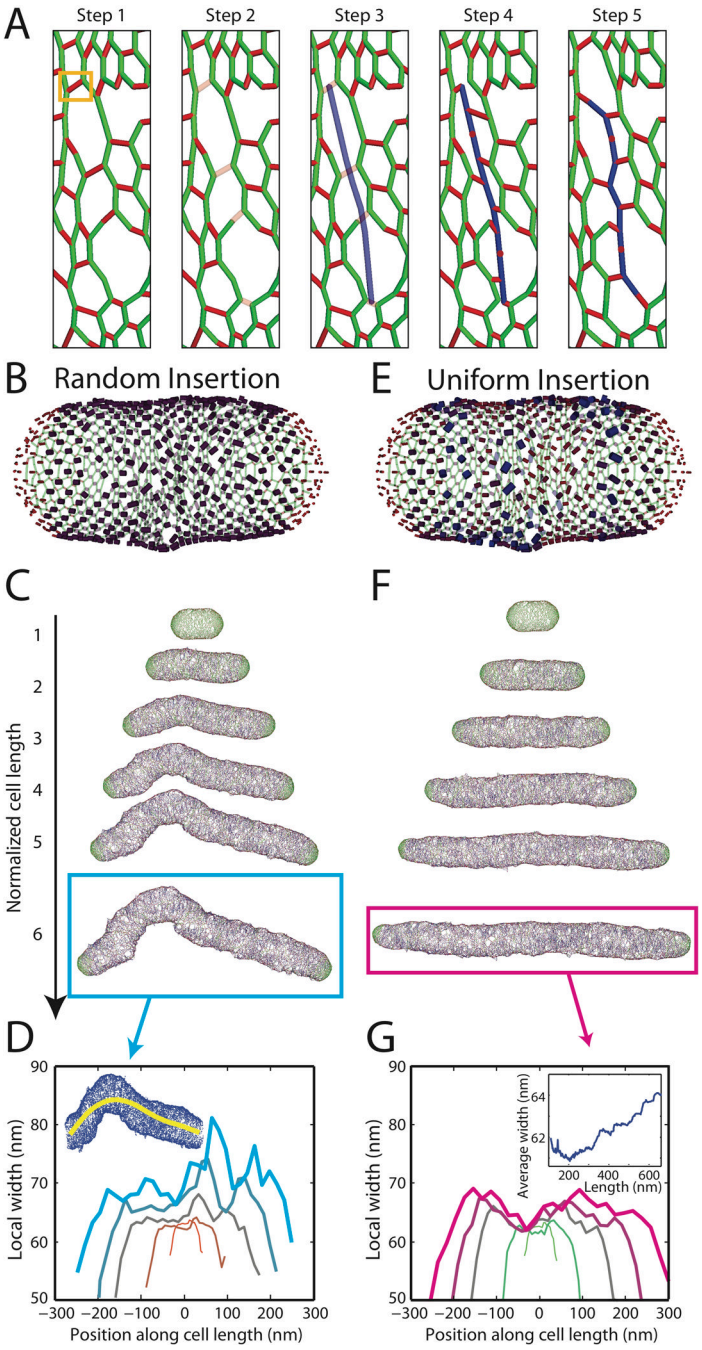

Figure 2. Cell shape is maintained by uniform peptidoglycan insertion

(A) Schematic of insertion steps for new glycan strands: (1) An existing peptide crosslink (boxed in orange) is chosen as the insertion starting point (glycans shown in green, peptides in red); (2) Peptides are removed from the adjacent glycan strands until the free path exceeds a defined length; (3) a new glycan strand (blue) is inserted; (4) glycan disaccharide subunits are crosslinked to nearby uncrosslinked glycans (red dots on the new strand indicate peptides that are too far to form crosslinks); (5) the new network is relaxed to its lowest energy state. (B,E) Schematic of random (B) and uniform (E) insertion models, with blue shading and peptide thickness indicating likelihood of selection as insertion site. (C,F) Cell walls grown *in silico* to six times their original length. (C) When new insertion sites are

chosen at random along the surface, severe bending and bulging results. (F) Uniform azimuthal and longitudinal density of insertion-site selection maintains rod shape. (D,G) Local width relative to the cell midline for cells shown in C,F. Line thickness is proportional to cell length. Inset in D shows the cell midline for the cyan-boxed cell in C. Inset in G shows the average width during elongation of the cell in F.

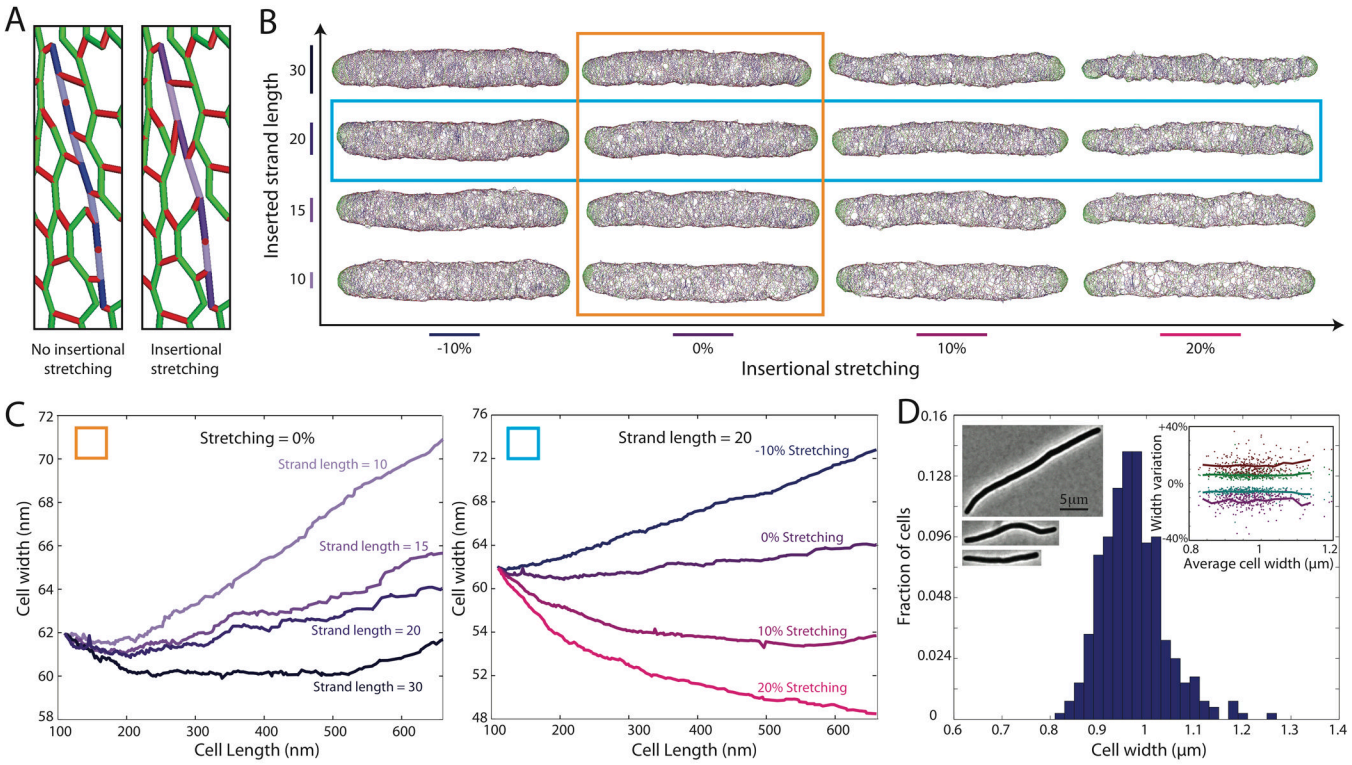

Figure 3. Cell width decreases as strand length and/or insertional stretching is increased

(A) Schematic of insertional stretching: Stretching of new strands before relaxation (purple) results in fewer glycan subunits per unit length. (B) Cell walls grown with uniform insertion to three times their original length, with insertional stretching ranging from −10% (i.e., compression) to +20% (*x*-axis) and inserted strand lengths ranging from 10 to 30 (*y*-axis). (C) Average local width as a function of length for (left) cells in orange column of B with different strand lengths and 0% insertional stretching and (right) cells in cyan row in B with different levels of insertional stretching and *L*=20 (blue row in B). The width remains constant as the cell wall elongates for strands of length 20 with 10% insertional stretching. (D) Local width remains roughly constant (0.97±0.07 μm, 312 cells) in filamentous *E. coli* K12 cells treated with cephalexin. Left insets: phase-contrast micrographs of typical cells (Scale bar: 5 μm). Right inset: Scatter plot of width variability within single cells, similar to Fig. 1B,C.

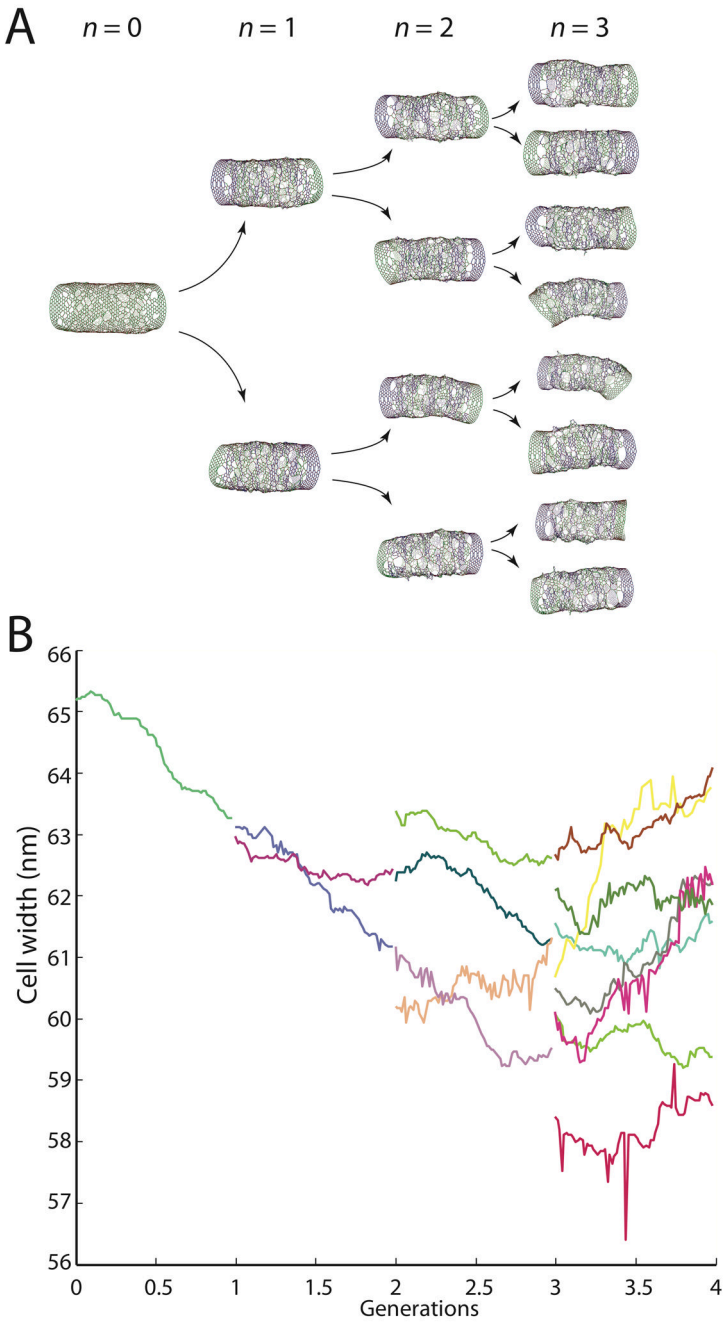

Figure 4. Cell width is preserved across multiple cycles of growth and division

(A) Model cells elongated using the uniform insertion model with L=20 and 10% stretching are divided in half after each doubling of cell-wall material. The cell wall networks for the first three generations are shown. (B) Average width for each of the cells in A, with each color representing a different cell. The cell-to-cell variability in width among the final eight cells is ~5%.

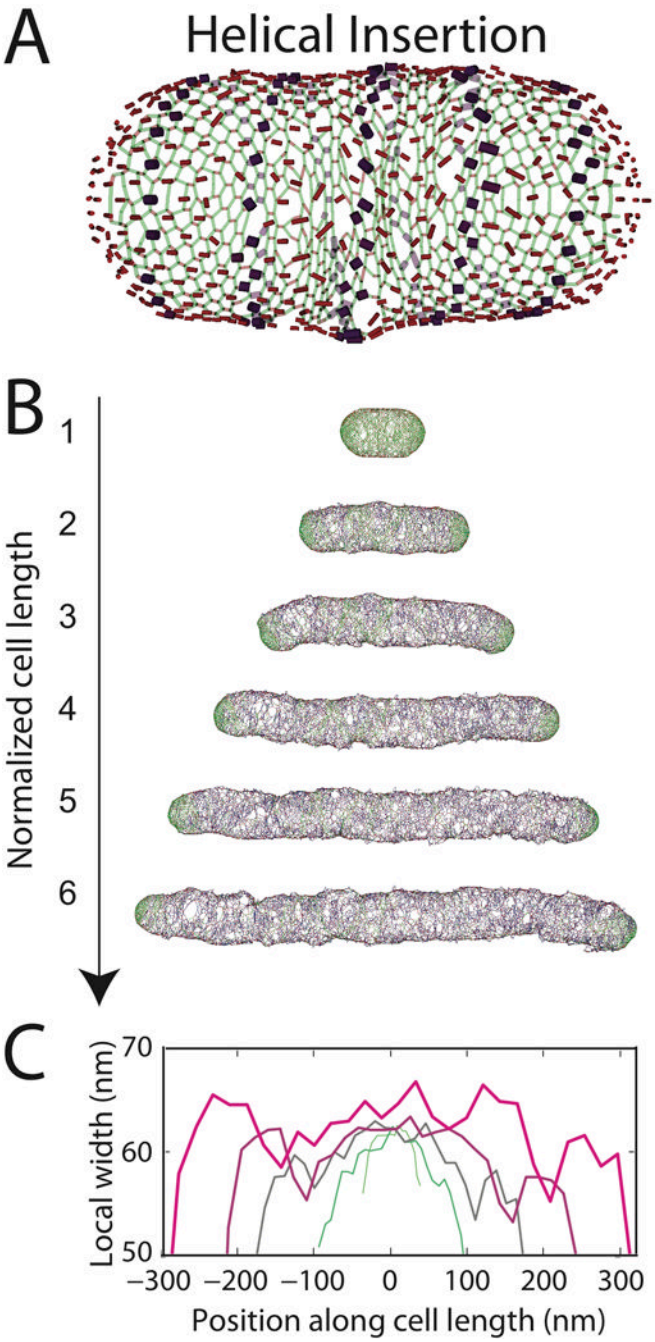

Figure 5. Cell shape is maintained with a helical pattern of insertion

(A) Schematic of helical pattern of insertion sites on the same model cell wall as in Fig. 2B,E. (B) Cell wall grown to six times its original length. (C) Local width of cell walls in B.

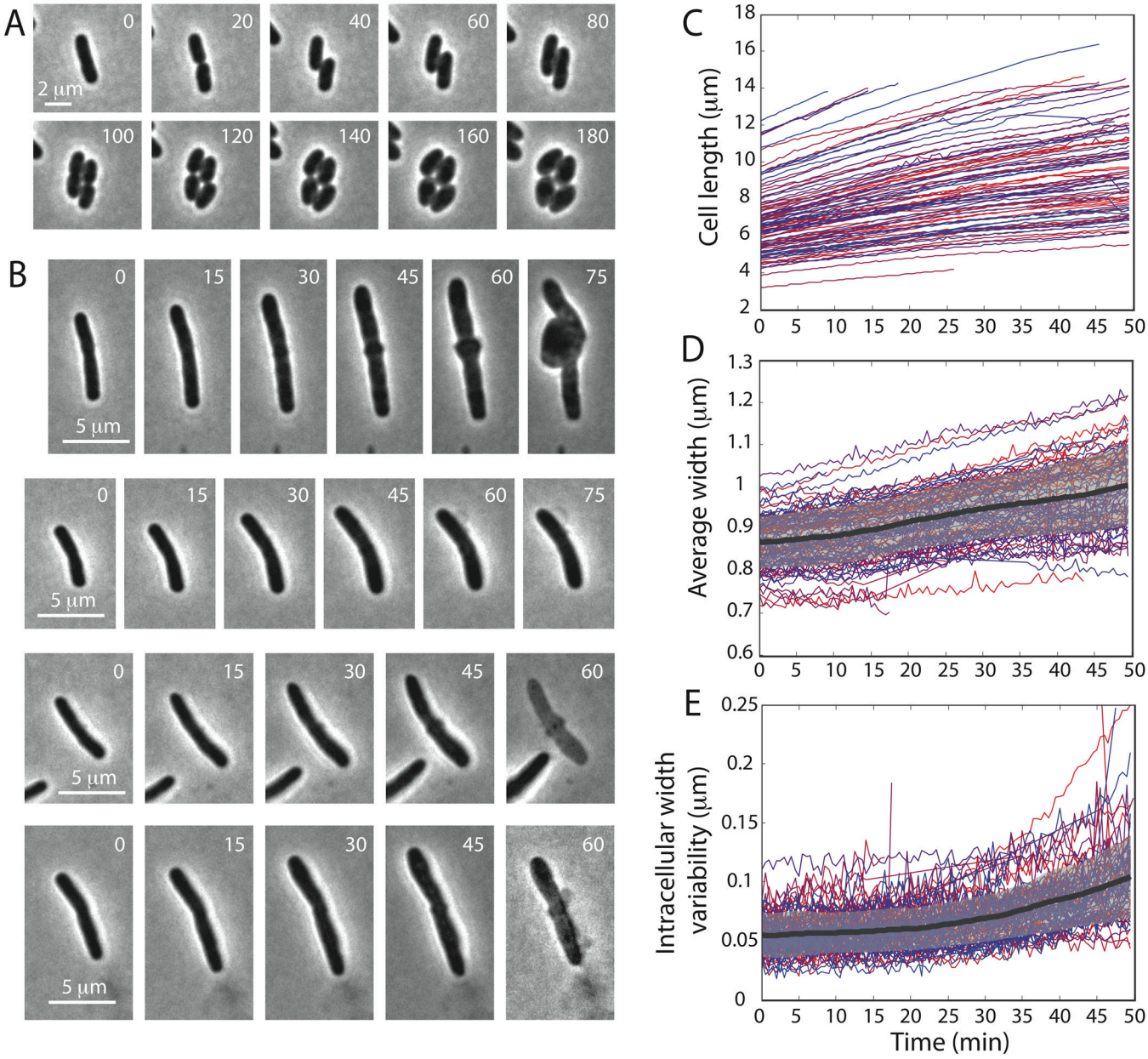

Figure 6. *E. coli* cells grown in the presence of cephalexin and A22 elongate with loss of rod-shape maintenance

(A) At least two rounds of cell division are required before A22-treated cells lose their rod shape. (B) After 60 minutes of growth in the presence of cephalexin, cells treated with A22 continue to elongate but width becomes more variable and cells eventually form bulges and then lyse. (C) Length as a function of time for 102 individual cells. Cells are color-coded identically in C–E. (D) Average cell width as a function of time. Thick black line indicates the population mean and gray region indicates one standard deviation above and below the mean. (E) Intracellular width standard deviation as a function of time. Thick black line indicates the population variability mean and gray region indicates one standard deviation above and below the mean. Time in minutes is shown in upper right.

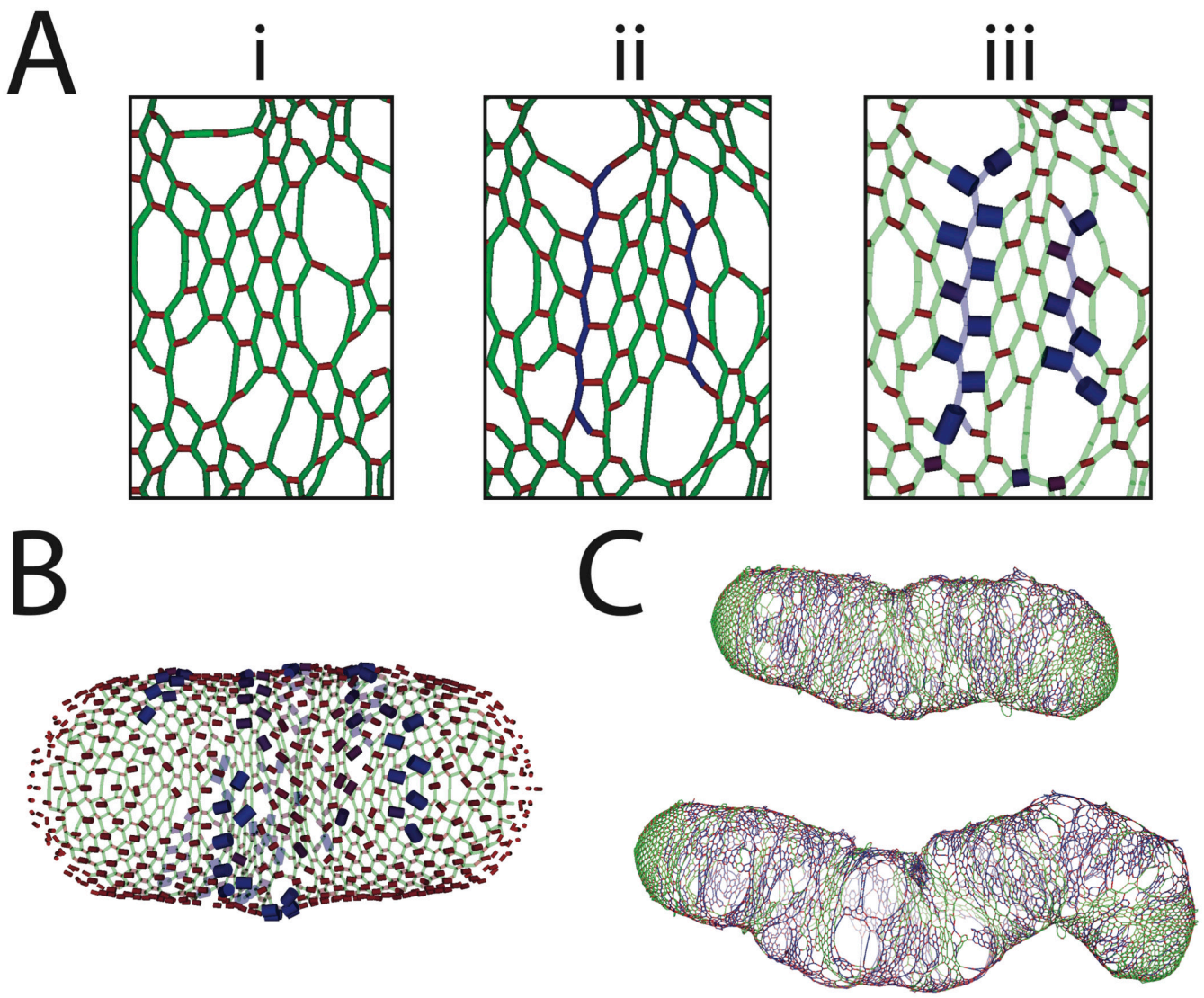

Figure 7. Tension-sensitive insertion causes rapid loss of cell shape

(A) Schematic of likelihood of initiation surrounding a recently inserted glycan strand based on tension-sensitive insertion. (*i*) Initial network before insertion, (*ii*) relaxed network after the insertion of two new strands (blue), (*iii*) peptides with largest tension highlighted by increased width and blue shading. (B) Schematic of likelihood of initiation across the cell wall, with increased insertion probability at crosslinks with highest tension. (C) Cell wall grown to two- and three-fold its original mass, with significant bending and increases in local width. After three-fold growth, the cell wall has almost completely lost its rod shape.